Chapter 7
Magnetic Properties of Small, Deposited 3d Transition Metal and Alloy Clusters

Michael Martins, Ivan Baev, Fridtjof Kielgast, Torben Beeck, Leif Glaser, Kai Chen and Wilfried Wurth

Abstract Clusters are structures in the nano- or sub-nanometer regime ranging from a few atoms up to several thousand atoms per cluster. Supported metal clusters and adatoms are interesting systems for magnetic studies as their magnetic properties can strongly depend on the size, composition and the substrate due to quantum size effects. This offers rich possibilities to tailor systems to specific applications by choosing the proper size and composition of the cluster. In this article the magnetic properties of small 3d metal and alloy clusters in the few atom limit measured by X-ray magnetic circular dichroism and how their spin and orbital moments depend on size and composition are discussed. Special emphasis is put on the non-collinear magnetic coupling in the clusters resulting in complex spin structures and the influence of oxidation on the magnetic properties of the clusters.

7.1 Introduction

When thinking about magnetism usually ferromagnetic coupling is considered, a phenomenon known for a long time. Since its discovery it plays an important role in various areas of technology, e.g., navigation or nowadays to store information. In a ferromagnetically coupled material the magnetic moments of the individual atoms within a domain are all oriented parallel to each other. However, there is also antiferromagnetism, with antiparallel orientation of the magnetic moments and more complicated magnetic structures, for example spin spirals [1, 2]. The coupling of a ferromagnet and an antiferromagnet can result in new effects such as the giant magneto-resistance observed in Cr-Fe multilayers [3–5]. Nevertheless, even more complex magnetic ordering exists, which is known from domain walls, showing a non-collinear coupling of the magnetic moments. Furthermore, in recent years another very complex type of non-collinear magnetic ordering has been observed, namely nano-scale magnetic skyrmions. These structures are topologically stabilized and may lead to new approaches for storing digital information [6]. As these

M. Martins (✉) · I. Baev · F. Kielgast · T. Beeck · L. Glaser · K. Chen · W. Wurth
Institut Für Experimentalphysik, Universität Hamburg, Hamburg, Germany
e-mail: michael.martins@uni-hamburg.de

© Springer Nature Switzerland AG 2018

R. Wiesendanger (ed.), *Atomic- and Nanoscale Magnetism*, NanoScience and Technology, https://doi.org/10.1007/978-3-319-99558-8_7

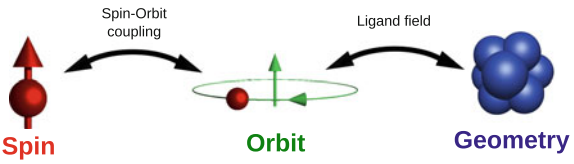

Fig. 7.1 Principle of the spin-lattice coupling in clusters and solids. Creative Common Attribution 3.0 License in J. Phys. C 28, 503002 (2016)

skyrmions can have very small sizes in the nm or even sub-nm regime, they may have potential as ultra-high density storage devices.

Nowadays, storing huge amounts of digital information in magnetic storage devices is still performed using small ferromagnetic domains. By decreasing the size of the magnetic particles storing the information enormous progress has been made in the last decades in increasing the available magnetic storage density. However, by decreasing the size of the particles further they will become superparamagnetic, i.e., the magnetic moments of the individual atoms in the particle are still ferromagnetically coupled, but the resulting total magnetic moment of the particle can rotate freely. The energy barrier which has to be overcome to rotate the magnetisation from the easy axis to another direction, e.g., switching from zero to one, is given by the anisotropy energy.

If information is stored in ferromagnetic particles the natural size limit is a single atom. Several studies have been performed on the magnetic properties of adatoms on different surfaces [7–15] and large anisotropy energies per atom have been found for some adatoms. However, a stable magnetisation of adatoms might have been observed recently for a single Holmium atom at cryogenic temperatures [8].

Magnetic particles with large magnetic moments and a sufficient anisotropy energy to store information at room temperature might be tailored by selecting a special number of atoms in the particle, e.g., using clusters with only a few atoms or magnetic molecules. As the physical and chemical properties of small clusters are strongly affected by quantum size effects these properties can strongly vary with the size even by removing or adding only a single atom ("each atom counts") [16], which has been shown for chemical [16, 17] as well as magnetic properties [18, 19] and opens a way to tailor the magnetic anisotropy. For this, the microscopic origin of the magnetic anisotropy in small clusters needs to be understood. In Fig. 7.1 the mechanism how the spin moment is coupled to the geometry via the spin-orbit coupling and the ligand field is sketched. The total magnetic moment of a cluster is mostly given by the spin moment of the atoms. As the spin has no direct coupling to the geometry of the cluster, the coupling of the magnetic moments must be mediated via the magnetic orbital moment of the atoms. The coupling to the spin is caused by the spin-orbit interaction. The orbital moment is coupled to the geometry of the cluster via the ligand or crystal field. As the ligand field is in general asymmetric, this asymmetry is transferred via the orbital moment to the magnetic spin moment, resulting in the magnetic asymmetry energy [20, 21]. Thus, the asymmetry might be enhanced by an increased spin-orbit coupling, a larger magnetic orbital moment or by a stronger ligand field. This mechanism has been demonstrated by

Gambardella et al. [7] for small Co adatoms and non size selected Co clusters on a Pt(111) surface. They found a clear correlation between the magnetic anisotropy energy per atom and the orbital magnetic moments of the Co atoms within the cluster.

Hence, experiments are mandatory which can measure both the spin and orbital magnetic moments of the supported clusters. Furthermore, experiments on such clusters have to be performed on mass selected clusters, as the magnetic properties can depend strongly on the exact number and geometry of atoms. Such experiments can be realised by X-ray spectroscopic methods like X-ray absorption (XAS) and especially X-ray magnetic circular dichroism (XMCD) spectroscopy [22]. Therefore, in this chapter the magnetic properties of mass selected, supported 3d transition metal and alloy clusters in the size range from the adatom up to a dozen atoms per cluster studied by X-ray magnetic circular dichroism will be discussed. A special emphasis is put on the non-collinear ordering in the small cluster and how non-collinear ordering is emerging or changing in small systems in the few atom limit. Furthermore, hybridization effects due to alloying of the clusters to tailor the orbital moments and the magnetic anisotropy will be discussed.

Small clusters are also interesting from a theoretical point of view, as they are large enough to show complex physical properties and small enough to use highly sophisticated theoretical methods. For a detailed understanding of their magnetic properties including the interaction within particles as well as with the substrate the systems should be studied also theoretically.

This chapter is structured as following. We will first discuss the experimental methods to produce and deposit mass selected clusters and will give a brief introduction on how to measure their magnetic properties using X-ray spectroscopy. As examples the magnetic properties of small Cr and Co clusters will be discussed. The influence of alloying Co clusters with 4d and 5d metals will be presented in the following section. Finally the influence of oxygen on the magnetic properties of Co and Co alloy clusters will be discussed.

7.2 Experiments

7.2.1 Cluster Sample Preparation

To perform X-ray spectroscopy on mass selected, supported metal clusters three steps are mandatory. The clusters have to be produced and subsequently mass selected, hence, the clusters should be produced as ions for an easy mass selection. Finally, the clusters have to be deposited on a substrate. In Fig. 7.2 the setup used in our experiment is sketched, consisting of cluster production, mass selection and deposition as well as spectroscopic investigation.

Within our setup [23], Xe ions with up to 30 keV kinetic energy are used to sputter a target with the cluster material put on high voltage. Atomic and cluster ions produced due to the sputtering process are accelerated typically to 500 eV kinetic energy and

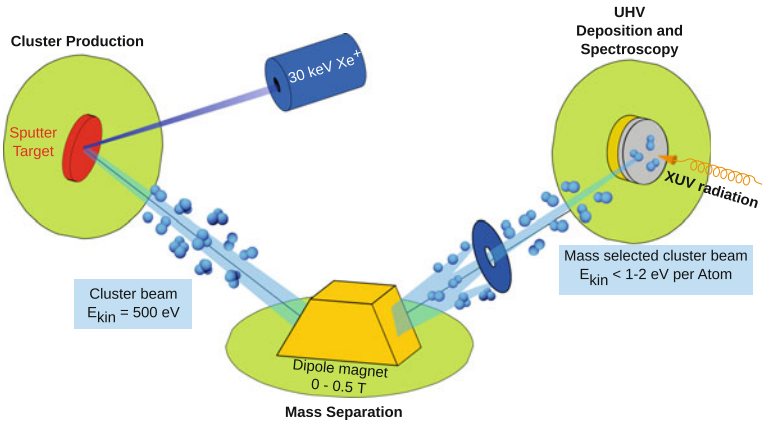

Fig. 7.2 Experimental setup for X-ray spectroscopy of deposited, mass selected clusters. Creative Common Attribution 3.0 License in J. Phys. C 28, 503002 (2016)

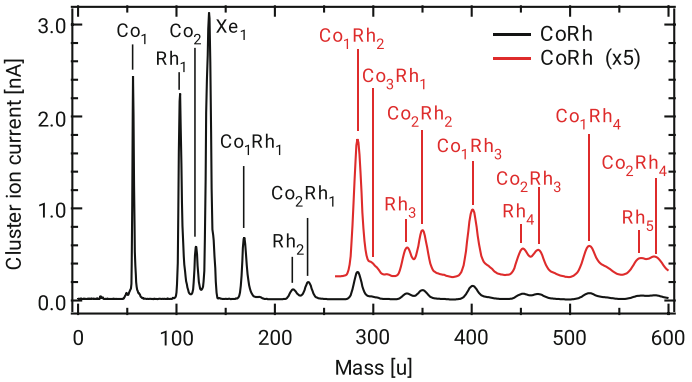

Fig. 7.3 Mass separated ion yield from a CoRh target produced by the ICARUS cluster source [23]. Creative Common Attribution 3.0 License in New J. Phys. 18, 113007 (2016)

are collimated by an electrostatic lens system. As the source is operated at a Xe background pressure around $1 \cdot 10^{-7}$ mbar with a base pressure of $\cong 1 \cdot 10^{-8}$ mbar or better the contamination of the often highly reactive small cluster ions with oxygen can be largely avoided. A typical example for the clusters which can be produced by the source is depicted in Fig. 7.3 for a CoRh alloy target. With increasing cluster size the yield is strongly decreasing. However, special size effects for some specific cluster sizes can increase the yield.

The mass selection of the clusters is achieved using a dipole magnet field. In particular for bimetallic alloy clusters a good mass resolution is required to select a specific size and composition. Here also the natural isotope distribution of the elements has to be taken into account, as this can strongly reduce the achievable

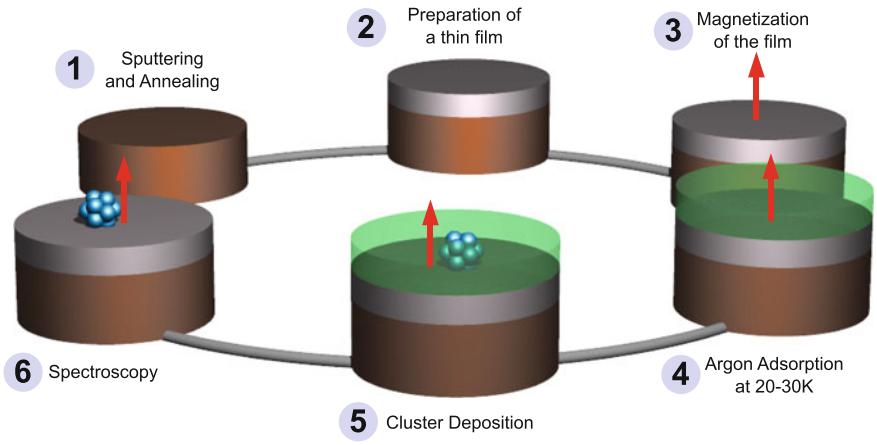

Fig. 7.4 Preparation of samples with mass selected clusters using the soft landing scheme described in the text. Creative Common Attribution 3.0 License in J. Phys. C 28, 503002 (2016)

mass resolution. From the measured ion current the density of the clusters on the surface can directly be calculated, if the size of the cluster spot is known.

To investigate the size dependency of the cluster properties, the coalescence or the interaction of the mass selected supported clusters have to be avoided. This can be realised by depositing only a small amount of clusters in the order of a few percent of a monolayer on the surface. However, to achieve a sufficient count rate in X-ray spectroscopy, a reasonable number of particles is required. The typical coverage given by the atom density in our experiments is on the order of 3% of a monolayer.

To deposit the metal clusters on a surface without fragmentation or changing the surface a soft landing scheme is used. Within this soft landing scheme the mass selected cluster ions are decelerated to a kinetic energy around 1 eV per atom. By using a rare gas buffer layer on the substrate of typically 5–10 monolayers the remaining kinetic energy of the clusters can be efficiently transferred to this buffer layer which is partially desorbed. Finally the rare gas layers are desorbed by flash heating the sample and the deposited clusters are in contact with the surface. Using molecular dynamics simulations Cheng and Landman [24, 25] have shown, that by this procedure, metal clusters can be landed on a surface without destruction.

The scheme to prepare the cluster samples in situ is depicted in Fig. 7.4. A Cu(100) single crystal is cleaned and prepared by sputter and anneal cycles (1). The clusters are deposited on thin magnetic films to align the cluster moments, prepared in the second step (2). In a third step (3) the films are out-of-plane magnetised to remanence. The clusters are deposited in the soft landing scheme in a thin noble gas layer of typical 5–10 monolayers (ML) (4) and the clusters are landing in the noble gas matrix with a kinetic energy less than 1 eV per atom (5). With typical retarded cluster currents between 10 pA up to 1 nA for the different cluster sizes the deposition process takes 5–60 min for a cluster coverage around 3% of a monolayer.

In a last step (6) the clusters are brought in contact with the surface by desorbing the noble gas layer by flash heating the sample to 80–100 K. The typical size of the cluster spot on the surface is in the order of 1–2 mm^2, which has then to be aligned to the synchrotron radiation beam.

7.2.2 X-Ray Absorption and Magnetic X-Ray Spectroscopy

Near edge X-ray absorption spectroscopy (NEXAFS) has been shown to be very sensitive to the electronic structure and by using circular polarised light also to the magnetic structure of the excited atoms [22, 26, 27].

Due to its element specificity X-ray absorption spectroscopy is well suited to study the electronic and magnetic properties of small, deposited clusters. The localised core electrons are excited into the unoccupied valence states and due to the dipole transition selection rules are excited to first order valence states with a specific angular moment. In Fig. 7.5b this excitation is sketched for the 3d metals, where the spin-orbit split $2p_{3/2}$ and $2p_{1/2}$ core electrons are excited into exchange split unoccupied 3d states.

To study dilute systems, such as submonolayer systems, a high intensity, stable and tunable X-ray source is required which can be produced by using undulators at third generation storage ring facilities [28]. Especially APPLE II [29] like undulator sources have been proven to be excellent sources for circular polarised synchrotron radiation over a wide energy range covering in particular L_{23}-edges of the 3d transition metals. In Fig. 7.5a the principle measurement scheme used in our experiments is depicted. The sample with the deposited clusters is magnetised out-of-plane and X-ray spectroscopy is carried out at normal incidence. The X-ray absorption is measured by recording the total electron yield via the sample current.

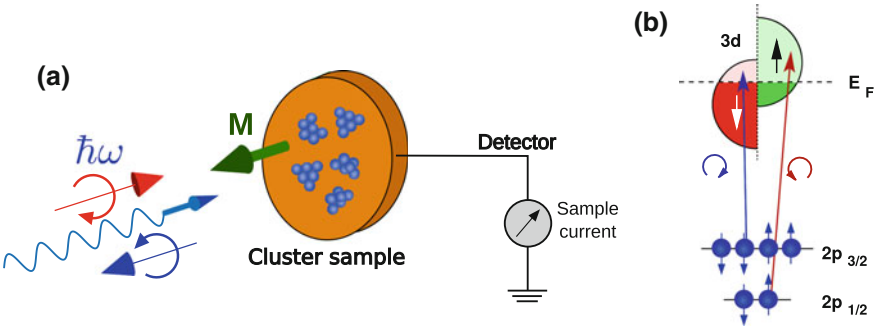

Fig. 7.5 Principle of X-ray and magnetic X-ray absorption spectroscopy. Exciting the spin-orbit split 2p electrons of a 3d metal atom of a magnetised sample with left and right polarised light (**a**) will create spin-polarised electrons, which probe the exchange coupling split empty *d* states (**b**). Creative Common Attribution 3.0 License in J. Phys. C 28, 503002 (2016)

Magnetic X-ray spectroscopy using circular polarised synchrotron radiation (XMCD) is especially useful to measure the spin and orbital magnetic moments which can be estimated using the sum rules [30, 31] given in (7.1) and (7.2) for $2p \rightarrow 3d$ transitions.

$$\mu_{\mathrm{S}}^{\mathrm{eff}} = -2\mu_B \cdot n_h \frac{A - 2B}{C} + T_z \tag{7.1}$$

$$\mu_\ell = -\frac{4}{3}\mu_B \cdot n_h \frac{A + B}{C} \tag{7.2}$$

with

$$C = C_{L3} + C_{L2} \tag{7.3}$$

A and B are the integrated dichroism signals at the L_3 and L_2 edge marked in Fig. 7.6, respectively. The normalizing factor C is the integrated intensity C_{L3} and C_{L2} over the L_2 and L_3 white lines, respectively. n_{h} is the number of d holes. For bulk materials this number is usually quite well known, however, it is not known for small clusters, where n_{h} might also change with the size of the cluster. Hence, all magnetic moments given are divided by n_{h}. The effective spin moment $\mu_{\mathrm{S}}^{\mathrm{eff}}$ includes the term T_{z} which is a magnetic dipole term and is a measure of the asphericity of the spin magnetisation [22]. In a system with cubic symmetry this term is in general negligible, but this does not hold for clusters and adatoms deposited on surfaces [7, 22, 32, 33] and the given spin moments $\mu_{\mathrm{S}}^{\mathrm{eff}}$ always include this usually unknown contribution.

The absolute spin and orbital magnetic moments can be estimated for the later 3d elements (Fe, Co, Ni) with an error around 10% [34]. For the other 3d elements, the error for the absolute value can be 50% or above, as the 2p spin-orbit splitting is decreasing and the L_3 and L_2 white lines start to overlap [35–37]. However, relative changes between different systems, e.g., different cluster sizes, of the magnetic moments can still be obtained.

In X-ray absorption spectra also the direct, non-resonant excitation into s-like states is included. This does not contribute to the magnetic properties, shows no resonant feature and can be described by a step function. In Fig. 7.6 X-ray absorption spectra of Fe_7 clusters deposited on a magnetised Ni/Cu(100) substrate are shown as an example. The L_3 and L_2 white lines at 708 and 720 eV due to the excitation of $2p_{3/2}$ and $2p_{1/2}$ electrons into unoccupied states are situated on a slowly varying background from the Ni/Cu substrate.

7.3 3d Metal Cluster

In the following section the magnetic properties of small chromium and cobalt clusters deposited on thin magnetised films will be discussed. Cr and Co have been

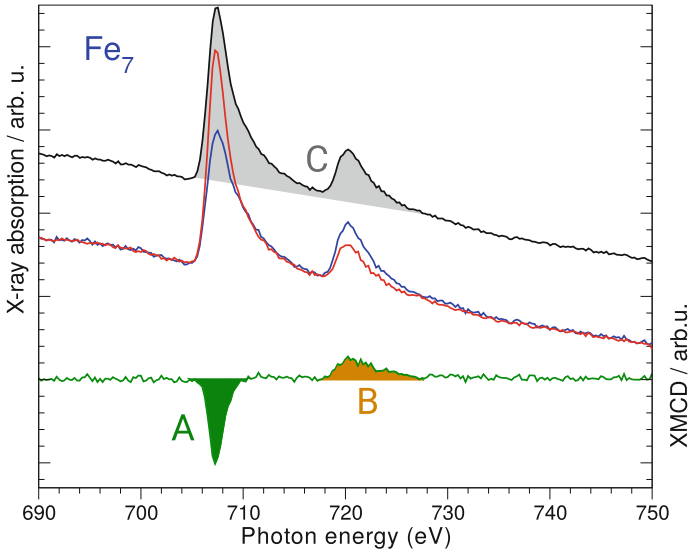

Fig. 7.6 X-ray absorption and magnetic circular dichroism (XMCD) spectrum of Fe_7 clusters deposited on an out-of-plane magnetised Ni/Cu(100) substrate. The red and blues curves are the X-ray absorption spectra recorded with the two light helicities. The upper (black) trace is the average absorption spectrum corresponding to the absorption of unpolarised or linear polarised light. The low (green) trace is the difference spectrum of both helicities, e.g., the XMCD spectrum. The shaded areas A, B and C are the areas used in the sum rules in (7.1) and (7.2). Creative Common Attribution 3.0 License in J. Phys. C 28, 503002 (2016)

chosen as examples for materials showing an antiferromagnetic and ferromagnetic coupling in the bulk, respectively.

7.3.1 Chromium Clusters

The clusters discussed in this chapter are in general too small for complex spin structures like skrymions, however, already a dimer on a magnetised surface might show a complex non-collinear magnetic coupling, if the magnetic coupling relative to the surface and within the dimer is antiferromagnetic. In Fig. 7.7 the possible magnetic structure for such adatoms and dimers deposited on a magnetised surface are depicted. For the dimer a ferromagnetic, an antiferromagnetic as well as a non-collinear coupling might be realised depending on the coupling strength between the adatoms J_{aa} and an adatom and the surface J_{as}.

Such ultra small non-collinear spin structures can be realised with chromium clusters, as chromium is a prototype system for an antiferromagnetic coupling in the bulk.

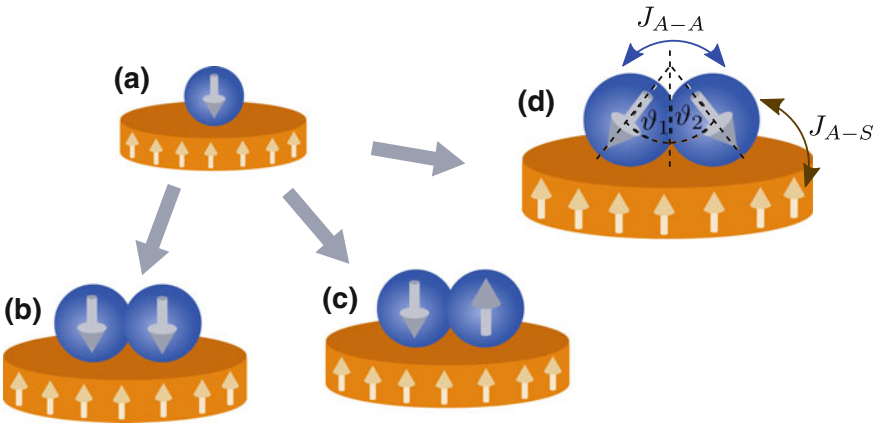

Fig. 7.7 Schematic illustration of the possible non-collinear coupling of a dimer on a magnetised surface. **a** antiferromagnetic coupling to the substrate of the adatom, **b** ferromagnetic coupling of the dimer, **c** antiferromagnetic coupling of the dimer, **d** non-collinear coupling of the dimer with angles $\vartheta_{1,2}$ and exchange coupling constants $J_{\mathrm{A-A}}$ and $J_{\mathrm{A-S}}$

In Fig. 7.8 the XMCD spectra of Cr adatoms and Cr_n clusters for $n = 3, 4$ deposited on a magnetised three monolayer Fe film, deposited on Cu(100) are depicted [38]. A strong XMCD signal is found, which shows a double peak structure at the L_3 edge. As the positive part is much stronger in total this XMCD signal corresponds to the expected antiferromagnetic coupling. This double peak structure is identical to the structure found for polarised Cr atoms in the gas phase by Prümper et al. [39]. In the gas phase the two peaks with opposite sign can be assigned to two different spin configurations of the 3d electrons, e.g., a ^7P and a ^5P multiplet [40].

The spin and orbital magnetic moments in the size range from the Cr adatom up to 13 Cr atoms per cluster deposited on a magnetised Fe film are depicted in Fig. 7.9. The orbital moment is close to zero and the spin moment is strongly decreasing from 0.4 μ_{B} for the Cr adatom down to 0.10–0.15 μ_{B} for Cr_n with $n \geq 8$. This strong decrease is a result of the increasing antiferromagnetic ordering of the Cr cluster with increasing size. The almost vanishing orbital moment for chromium can be attributed to the d^5 high spin configuration, which will have a total angular momentum $L = 0$ according to the Pauli principle.

From Fig. 7.7 for a Cr dimer on a magnetic surface already a non-collinear spin structure is expected, which would result in a strongly reduced magnetic moment. However, the magnetic moment is only slightly reduced compared to the Cr adatom suggesting a ferromagnetic coupling of the Cr atoms in the dimer coupled antiferromagnetically to the substrate shown in Fig. 7.7b.

The exchange coupling J between the Cr adatoms $J_{\mathrm{A-A}}$ and the Cr atoms and the Fe substrate $J_{\mathrm{A-S}}$ has been calculated in [38] using the SPR-KKR (spin-polarised relativistic Korringa–Kohn–Rostoker) method. The classical spin Hamiltonian is given by

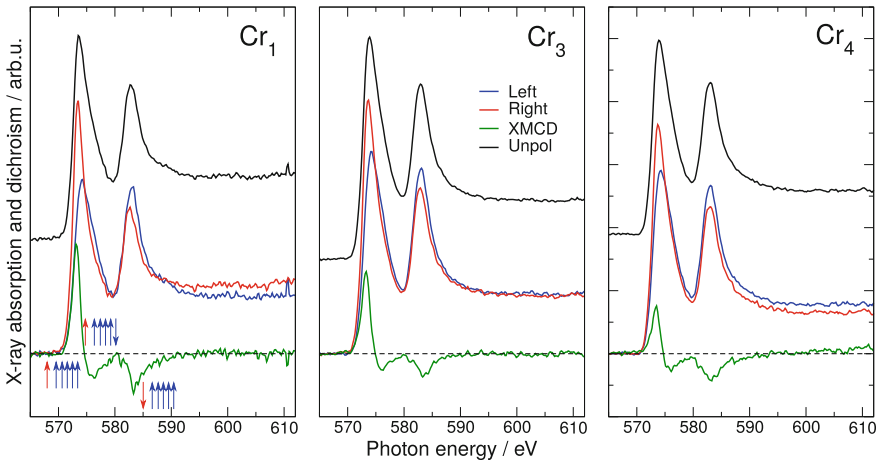

Fig. 7.8 X-ray absorption and XMCD spectra for different $Cr_{1,3,4}$ clusters deposited on a Fe/Cu(100) surface. The arrows in the Cr_1 graph depict the spin of the 2p core hole (red) and the 3d electrons (blue). The dashed line is the zero line for the XMCD as well as the left and right polarised XAS spectra. The unpolarised spectrum is shifted up for convenience. Creative Common Attribution 3.0 License in J. Phys. C 28, 503002 (2016)

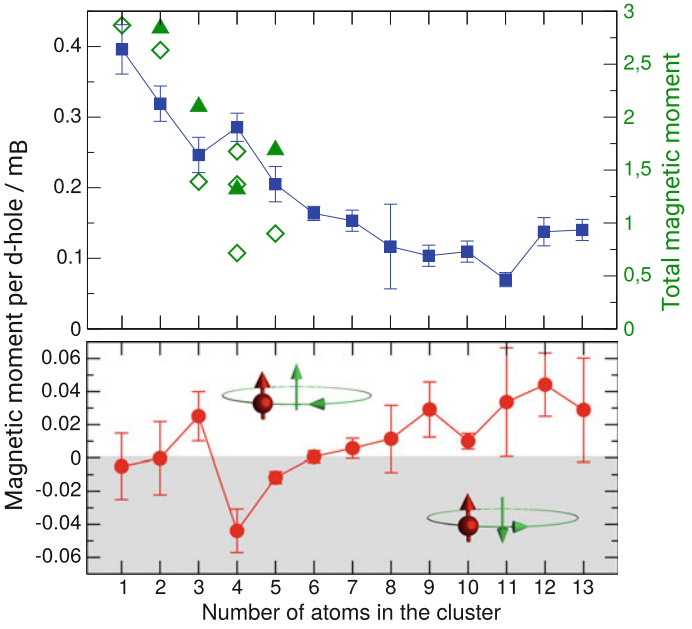

Fig. 7.9 Experimental magnetic spin μ_s (■) and orbital μ_ℓ (●) moments of chromium adatoms and small clusters in the mass range from n = 1 − 13 on a Fe(100) fcc surface. Theoretical total magnetic moments from [38] (◇) and [41] (▲). Note the different y-scales on the graphs. Creative Common Attribution 3.0 License in J. Phys. C 28, 503002 (2016)

$$\mathcal{H} = -\frac{1}{2}\sum_{i \neq j} J_{ij} e_i e_j, \tag{7.4}$$

where $e_{i,j}$ is a unit vector defining the direction of the magnetic moment and i and j indicate the Cr cluster atoms and their first Fe neighbors. Taking into account only first-neighbor interactions and neglecting the rotation of Fe moments the Hamiltonian for the Cr dimer can be described by

$$\mathcal{H} = -J_{A-A}\cos(\vartheta_1 + \vartheta_2) - 4J_{A-S}(\cos\vartheta_1 + \cos\vartheta_2), \tag{7.5}$$

with $\vartheta_{1,2}$ the angle of the Cr magnetic moments relative to the magnetisation of the Fe substrate (see Fig. 7.7). The angle defining the non-collinear solution can be obtained by minimizing (7.5) as

$$\cos(\vartheta_1) = \cos(\vartheta_2) = -2J_{A-S}/J_{A-A}. \tag{7.6}$$

If $2|J_{\mathrm{A-S}}| > |J_{\mathrm{A-A}}|$, the angle is not defined and the non-collinear solution does not exist. For Cr_2 on the Fe substrate this is realised, as $2|J_{\mathrm{Cr-Fe}}| = 2 \times 80.8\,\mathrm{meV} > |J_{\mathrm{Cr-Cr}}| = 77.6\,\mathrm{meV}$.

Hence, the exchange coupling of the individual Cr atoms to the Fe substrate is much stronger in comparison to the Cr–Cr coupling. This results in a ferromagnetic coupling of the two Cr spins which are then coupled antiferromagnetically to the Fe surface as depicted in Fig. 7.7d.

In Fig. 7.10 the calculated spin orientations for a Cr trimer and two possible geometries of Cr tetramers are depicted. A non-collinear coupling is found for all clusters. However, for the structure of Cr_4 the non-collinear coupling is less pronounced. Starting from Cr_5 a transition to an antiferromagnetically coupled Cr cluster is continuing decreasing the non-collinear contributions.

In Fig. 7.9 the results for the experimental and calculated magnetic moments of Cr_n clusters on a 3 ML Fe/Cu(100) are compared. In the calculations a Fe(100) fcc surface has been used, as the 3 ML thick Fe film is growing pseudomorphically on a fcc Cu(100) surface. Only if a non-collinear coupling due to a spin frustration within the clusters is taken into account in the calculations the principle behaviour of the experimental data can be described. For the direct comparison of the experimental and theoretical total magnetic moment per atom the number of d-holes n_{d} is required in (7.1). Furthermore, for Cr the XMCD sum rules might be wrong by 50% for the absolute values [35–37]. Hence, in Fig. 7.9 the experimental spin moments and the theoretical total moments are compared on a relative scale.

The calculations of Robles and Nordström [41] in Fig. 7.9 are using a tight-binding model for the s, p and d valence electrons in a mean-field approximation. They have calculated the magnetic coupling and the total moments from the Cr dimer up to Cr_9 clusters taking into account a collinear and a non-collinear coupling of the individual magnetic moments. The calculated total moment of the clusters is always antiferromagnetically coupled to the fcc Fe(100) surface and the non-collinear

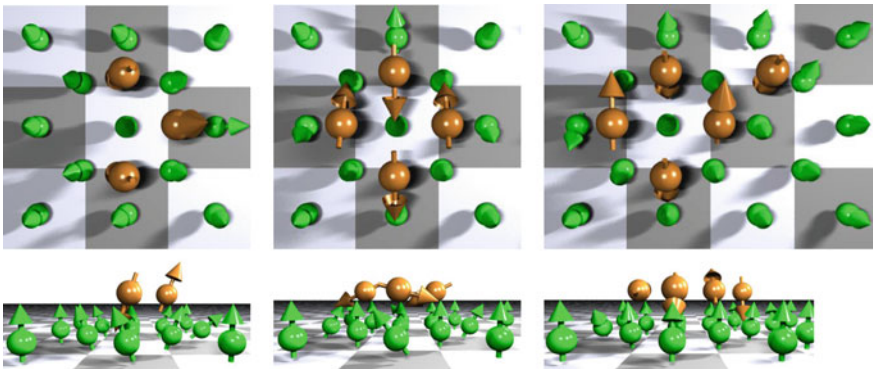

Fig. 7.10 Non-collinear coupling in small chromium clusters. Left: Cr trimer, middle: Compact Cr tetramer, right: Cr pentamer (from [38])

coupling results in a strong reduction of the magnetic moments with increasing cluster size similar to the experimental data and the SPR-KKR calculations. Robles and Nordström have also calculated the magnetic properties of Cr clusters on a bcc Fe(100) surface. The total moment of the clusters is also antiferromagnetically coupled to bcc Fe surfaces, however, with much larger magnetic moments.

Hence, the surface has a tremendous effect on the magnetic properties of the clusters, and further experiments of Cr adatoms, dimers and trimers deposited on a magnetised Ni/Cu(100) film have been performed. Only very small XMCD signals are found for all samples [42, 43], indicating an antiferromagnetic ordering relative to the magnetisation of the Ni substrate. Assuming as a first approximation a similar exchange coupling $J_{\mathrm{Cr-Cr}}$ for the Cr atoms in the dimer and a much smaller coupling of the Cr atoms to the Ni surface $J_{\mathrm{Cr-Ni}}$ compared to $J_{\mathrm{Cr-Fe}}$ above, (7.6) will give $\cos(\vartheta_{\mathrm{k}}) \approx 0$ and the magnetic moments in the Cr dimer on the Ni surface will be oriented almost perpendicular to the Ni magnetisation resulting in an almost vanishing dichroism signal measured perpendicular to the surface.

The magnetic structure of small Cr clusters on a magnetised Ni surface has been studied theoretically by Lounis et. al [44] using the SPR-KKR method. For the Cr dimer they find a large $J_{\mathrm{Cr-Cr}} \cong -200\,\mathrm{meV}$ exchange coupling compared to $J_{\mathrm{Cr-Cr}} \cong -77\,\mathrm{meV}$ for Cr on the Fe surface and a much weaker $J_{\mathrm{Cr-Ni}} \cong -5\,\mathrm{meV}$ exchange coupling to the surface. From that they calculate an antiferromagnetic ordering of the Cr spins with the collinear configuration as the ground state and the non-collinear state as a local minimum. Also for the Cr trimer on Ni/Cu(100) a collinear spin configuration parallel to the Ni magnetisation is predicted, which should show an XMCD signal in the experimental geometry. Here also a non-collinear solution perpendicular to the Ni magnetisation similar to the Cr dimer would explain the experimental result [43].

Using the orbital sum rule (7.2), the orbital moments μ_ℓ of the Cr clusters deposited on the Fe/Cu(100) substrate have been evaluated and are shown in the lower part of Fig. 7.9. Due to the half filled d shell the ground state of free Cr atoms is $^7S_3$

and thus the orbital moment $\mu_\ell = 0$. As expected, for the deposited Cr clusters very small orbital moments μ_ℓ close to zero are observed. The sign of the orbital moment represents the orientation relative to the spin moments, indicating a trend to a parallel coupling of the orbital and spin moments for larger clusters. This is in contrast to the data of Scherz et al. [36, 37], who found a very small orbital moment $\mu_{\ell,\text{film}} = -0.011\,\mu_\text{B}$ coupled anti-parallel to the spin moment for ultra-thin chromium films.

An interesting behavior is found for the Cr_3 and Cr_4 clusters. Cr_3 has a small orbital moment $\mu_{\ell,3} = 0.025(15)\,\mu_\text{B}$ parallel to the spin moment μ_S, whereas Cr_4 shows an orbital moment $\mu_{\ell,4} = -0.044(13)\,\mu_\text{B}$ with an anti-parallel coupling relative to the spin. This finding is already evident from the XMCD spectra of these clusters depicted in Fig. 7.8. Cr_4 shows a much weaker positive XMCD signal at the L_3 edge compared to Cr_1 and Cr_3, whereas the negative part at the L_3 edge and the XMCD signal at the L_2 edge is less affected. This change in the relative orientation of the spin and orbital moment with the cluster size can be explained by a small change of the number of d-holes n_d [43]. According to Hund's rule for a more than half filled shell the ground state of an atom has the maximum possible angular momentum J corresponding to a parallel coupling of the orbital and spin moment. However, for a less than half filled shell the situation changes and an anti-parallel orientation of orbital and spin moment is favored. The Cr atom with $3d^5$ has a half filled shell and the number of d-holes n_d of the Cr atoms in the clusters should be close to 5. However, a small deviation from 5 will result either in a parallel or anti-parallel coupling of the spin and orbital moments. Hence, within this simple model an increase of the number of d-holes would favor the observed anti-parallel coupling of orbital and spin moment in the Cr_4 cluster [43].

7.3.2 Cobalt Clusters

In Fig. 7.11 the magnetic spin and orbital moments for Co clusters deposited on a Ni/Cu(100) [45] and a Pt(111) [7] surface in the few atom limit are depicted. Size selected Co_n cluster with $n = 1 - 3$ have been studied on the remanently magnetised Ni/Cu(100) surface, whereas on the Pt(111) surface size averaged $Co_{\langle s \rangle}$ in a strong magnetic field has been investigated.

Spin and orbital magnetic moments are found to be larger on the Pt(111) surface compared to the Ni/Cu(100) surface. In particular for the Co adatom on Pt(111) a giant orbital moment is found, which is decreasing with increasing size $\langle s \rangle$. On the Ni/Cu(100) surface the smaller orbital moments show a non-monotonic behavior. They are decreasing from the adatom to the dimer, however, for the Co trimer the largest orbital moment is found. Hence, Co clusters show larger magnetic moments on the more weakly coupling Pt(111) surface. This might be attributed to the effect of hybridisation of the 3d orbitals with the substrate, which is in this case smaller with the filled Pt 5d band.

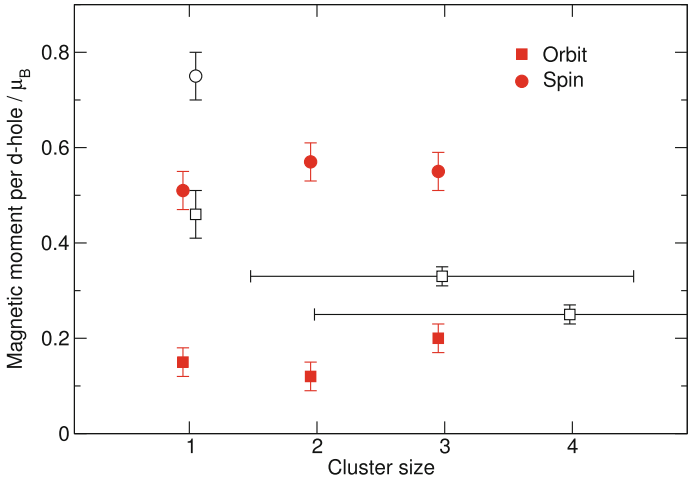

Fig. 7.11 Spin (circles ◯) and orbital (squares □) magnetic moments of small Co clusters on two different surfaces; filled symbols: mass selected Co_n on Ni/Cu(100), open symbols: size averaged $Co_{\langle s \rangle}$ on Pt(111) taken from [7] with the number of d-holes $n_d = 2.40$. Creative Common Attribution 3.0 License in J. Phys. C 28, 503002 (2016)

Co adatoms and dimers on a Ni surface show a similar size dependency as the corresponding Fe adatoms and dimers with a small increase of the spin moments [18, 19, 46]. The orbital moment is slightly decreasing from Co_1 to Co_2 and is almost equal for Fe_1 and Fe_2. Adding a further Co atom to dimer increases the orbital moment strongly by 50% while the spin moment for the Co_2 and Co_3 are rather similar. In contrast to this, adding an Fe atom to the Fe_2 the orbital and spin moment drops by 50 and 25%, respectively.

7.4 Alloy Clusters

Already for clusters with only one element a strong size dependency of the magnetic moments is found. However, to enhance or tailor the orbital and spin magnetic moments or tuning the magnetic anisotropy not only clusters consisting of one element should be taken into account. 3d metal atoms have a large spin moment, however, the spin-orbit interaction is rather small. In contrast to that the corresponding 4d and 5d elements as Rh or Pt have a larger spin-orbit interaction, but in the bulk are non-ferromagnetic. However, they can be polarised and small Rh clusters show a superparamagnetic behaviour in the gas phase [47]. Also for small Ru clusters on the Fe/Ni(100) substrate a magnetic ordering has been measured [48], whereas for Ru and Rh impurities on Ag(100) and Pt(997) no magnetic moments could be found [49].

3d/4d or 3d/5d metal alloys, as e.g. Co-Cr-Pt, FePt, CoPt are often planned or already used in modern magnetic storage devices [50–52]. These alloys are interesting for applications as the anisotropy energy might be enhanced by combining the large magnetic moments of the 3d metals and the large spin-orbit interaction of the 4d/5d metals. Therefore, the magnetic spin and orbital moments have been studied on size-selected alloy clusters depending on the exact size and composition.

For all deposited clusters the exact structure is in general not known and could not be easily measured, even if the clusters are produced by atom manipulation [53]. This becomes even more critical for alloy clusters, as the number of possible geometric configurations is further increased [43]. As the typical spot size of soft X-rays is in the order of some 10 μm only an average of these different structures will be measured. For the case of Cr_4 it has already been discussed above that different geometric configurations can show different magnetic properties.

7.4.1 Co Alloy Clusters

For Co clusters three different alloy systems, CoPt [45], CoPd [54] and CoRh [55], have been studied. In Fig. 7.12 the spin and orbital magnetic moments as well as the ratio of these quantities are depicted for some Co_nM_m alloy clusters together with Co_n ($n = 1 - 3$) clusters deposited on an out-of-plane magnetised Ni/Cu(100) substrate as described above. For both alloy clusters an increase of the orbital moment with increasing number m of 4d/5d atoms is found. For Co_2Pt also the spin moment is increasing, whereas for CoPd the spin moment is decreasing, which results in a strongly enhanced orbital to spin ratio for both systems.

Comparing the results for the Co and CoPt clusters to corresponding Co [56–58] and CoPt [59] nanoparticles as well as CoPt thin films [60, 61] slightly smaller spin moments within the small cluster are found. However, the orbital moments are strongly enhanced. Hence, the aim to increase the orbital moments anticipated by alloying 3d and 4d/5d can be achieved. Essential for this effect is the hybridisation of the 3d and the 4d or 5d electrons in an alloy cluster.

One should already note here that also the chemical reactivity of the Co clusters is strongly enhanced by alloying with the 4d and 5d metals atoms inhibiting experiments on other Co alloy clusters. This will be discussed further in Sect. 7.5.

7.4.2 FePt

To study the effect of the hybridisation of the 3d and 5d elements in more detail a study on Fe_nPt_m clusters has been performed by Chen et al. [46]. An important quantity to understand the magnetic coupling is the spin-orbit (SO) interaction of the 3d electrons as sketched in Fig. 7.1. The SO should be increased to potentially increase the orbital moments and, in turn, maybe the anisotropy energies per atom.

As has been shown by Thole and van der Laan [62, 63], the 3d spin-orbit interaction can be obtained from X-ray absorption spectroscopy by evaluating the branching ratio

$$B_r = \frac{C_{L3}}{C_{L3} + C_{L2}} \tag{7.7}$$

of the L_3 and L_2 white line intensities C_{Lx} defined in (7.3) and depicted in Fig. 7.6. The branching ratio B_{r} depicted in Fig. 7.13 is increasing with increasing Pt content, which is attributed to an increased 3d spin-orbit interaction of the Fe 3d electrons by hybridisation with the Pt 5d electrons.

In Fig. 7.14 the XMCD spectra, normalised to the same intensity at the L_2 edge, of Fe_2Pt_m clusters are shown. The L_3 XMCD lines have a similar height, however, with increasing number of Pt atoms in the cluster the L_3 XMCD line is getting narrower. This corresponds to a change of the unoccupied density of states of the clusters and is a result of the change in hybridisation. The spin and orbital moments calculated by the sum rules from (7.1) are shown in the left panel of Fig. 7.13. The orbital moment (□) of Fe_nPt_m is decreasing with increasing number m of Pt atoms and the spin moment (◯) has a maximum for $m = 1$ and is decreasing, if a second Pt atom is added. From this one can conclude, that there is an optimal number of Pt atoms in the Fe cluster to create the maximum spin moment. This is in contrast to FePt bulk, thin films and nanoparticles [64–66], where the effective spin moment is increasing with the Pt content up to about 50 at% Pt and is rather constant for larger Pt content [64].

From Fig. 7.13 an increase of the Fe 3d spin-orbit interaction with increasing Pt content has been concluded by Chen et al. [46]. However, this increase for the Fe_nPt_m

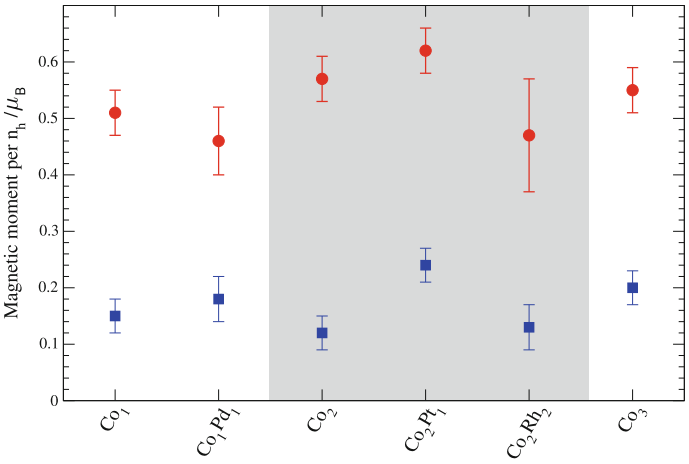

Fig. 7.12 Measured spin (•) and orbital (■) magnetic moments of Co_nM_m ($n = 1 - 3$) 3d metal alloy clusters depending on the size and composition of the cluster. Note, that the Co_2Rh_2 cluster has a ≈10% contribution from the oxidised cluster

clusters does result in a decrease of the orbital moment and an increase of the spin moment.

7.5 Magnetism and Chemical Reactivity

A critical point in the preparation of cluster samples is their possibly high chemical reactivity. In this section the chemical reactivity in terms of oxidation and its effect on the magnetic properties of the clusters will be discussed.

Using the setup described in Sect. 7.2.1 pure metallic alloy clusters with various compositions and sizes can be created. However, when the clusters are deposited in the noble gas matrix they might change their chemical state. The advantage of X-ray absorption spectroscopy in studying deposited clusters is its capability to get information about the chemical state of a 3d metal due to the varying multiplet structure.

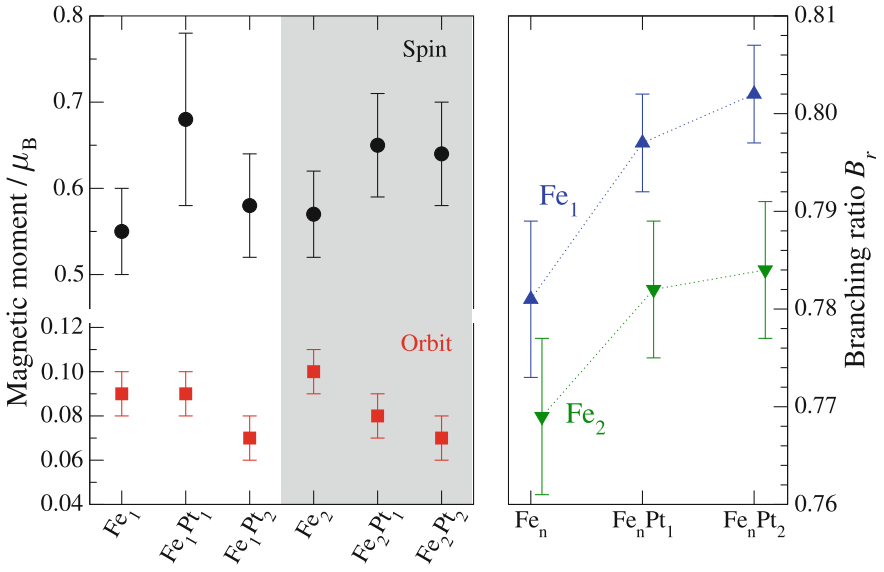

Fig. 7.13 (Left panel) Spin (●) and orbital (■) moments of Fe_nPt_m clusters deposited on a magnetised Ni/Cu(100) substrate; (right panel) Branching ratio B_r of the intensity of the L_3 and L_2 white lines for Fe adatoms, dimers and Fe_nPt_m clusters

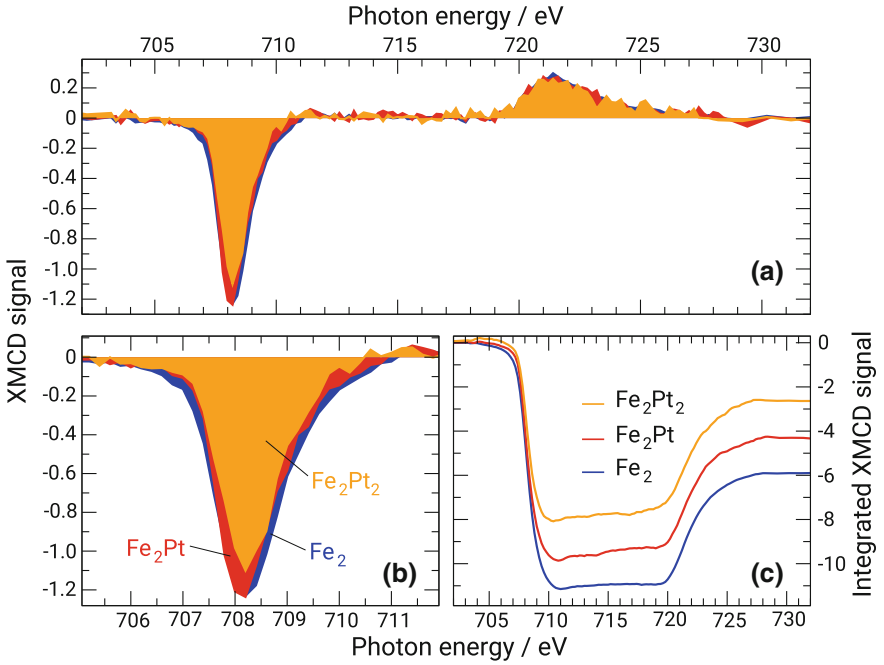

Fig. 7.14 Normalised (**a**) and integrated (**c**) L-edge XMCD spectra of Fe_2Pt_n clusters deposited on a magnetised Ni/Cu(100) surface. In **b** the normalised L_3 XMCD signal is enlarged. The XMCD spectra have been normalised to the integrated intensity of the L_2-edge. For Fe_2 and Fe_2Pt_1 the L_3 XMCD signal has the same height; however, the line shape of Fe_2Pt_1 is narrower, resulting in the observed decreasing integrated L_3 XMCD intensity in **c** by adding Pt to Fe_2. Creative Common Attribution 3.0 License in New J. Phys. 18, 113007 (2016)

7.5.1 CoO

As discussed in Sect. 7.3.2 Co clusters and Co metal show a ferromagnetic ordering. In contrast oxides such as CoO or NiO show an antiferromagnetic ordering. Hence, as a first system oxidised Co adatoms on a Ni/Cu(100) substrate will be discussed.

The pure Co metal clusters are not sensitive to oxidation and the X-ray absorption spectra of deposited clusters are usually varying only slightly with the cluster size. Usually the L_3 white line is shifting in energy but the shape is unchanged as has been shown, for the example, for Cr clusters in the size range from the adatom up to 13 atoms per cluster [67].

CoO was prepared by depositing Co cations in a noble gas matrix with a small amount of oxygen as described in [54]. A change in the oxidation state of a 3d metal can be monitored by the NEXAFS spectra at the L_3 edge, as depicted in Fig. 7.15. CoO shows a multiplet structure whereas non-oxidised Co adatoms and clusters show a metallic-like resonance. With this knowledge the oxidation state of the deposited clusters can be estimated [54]. In the right panel of Fig. 7.15 the X-ray absorption and

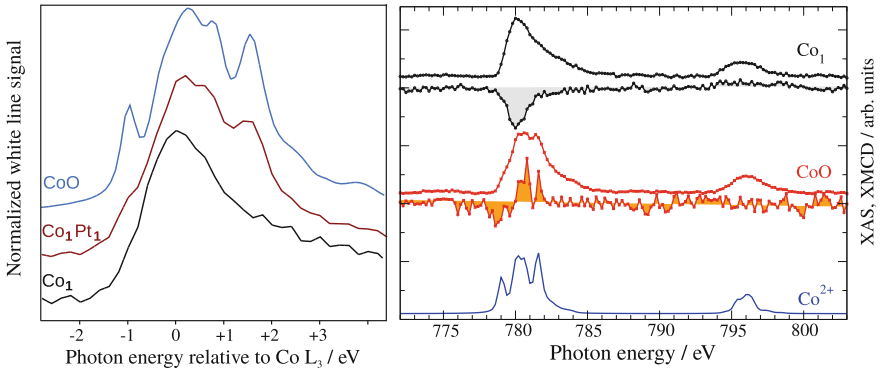

Fig. 7.15 (Left) L_3 XAS spectra of Co_1, Co_1Pt_1−O and bulk CoO; (right) XMCD and XAS spectra of Co_1 and CoO on Ni/Cu(100). The lower curve is the result of a multiplet calculation for Co^{2+}

XMCD spectra of CoO and the result of a multiplet calculation are depicted. The XAS spectrum clearly shows a multiplet structure similar to that of CoO. Compared to Co adatoms the XMCD signal is strongly suppressed and shows an antiferromagnetic ordering of the Co magnetic moment relative to the Ni substrate.

7.5.2 CoPd Dimers

In Fig. 7.16 the X-ray absorption and XMCD spectra of CoPd dimers on a magnetised Ni/Cu(100) film for different amounts of oxidation are depicted. From this data the XMCD spectrum of a pure oxidised CoPd-O cluster can be calculated as described in Chen et al. [54]. Similar as for CoO and for CoPdO an antiferromagnetic coupling is found, however with a magnetic spin moment $\mu_s^{\text{eff}} = -0.29(9)\ \mu_B$. For example, the spin moment in CoPd-O is only 30% compared to CoPd, but its orientation relative to the Ni magnetisation has changed.

7.5.3 CoRh Oxidised Clusters

The rather large number of stable Pd isotopes results in broad mass distributions of the different Co_nPd_m clusters which complicates the mass selection of clusters with a specific size and composition. Hence, Co_nRh_m clusters have been studied, as Co and Rh have only one natural stable isotope and a large number of specific compositions can be selected from the mass spectrum depicted in Fig. 7.3. Similar to the other Co_n 4d/5d alloy clusters also Co_nRh_m shows a strongly enhanced chemical reactivity.

For Co_1Rh_m ($m = 0, 1, 2$) an increase of the chemical reactivity with the number of Rh atoms in the cluster is found, as the amount of oxidised clusters on the surface

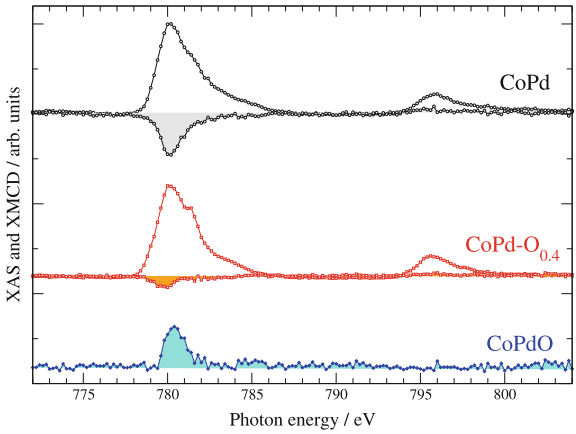

Fig. 7.16 XMCD and XAS spectrum of CoPd-O

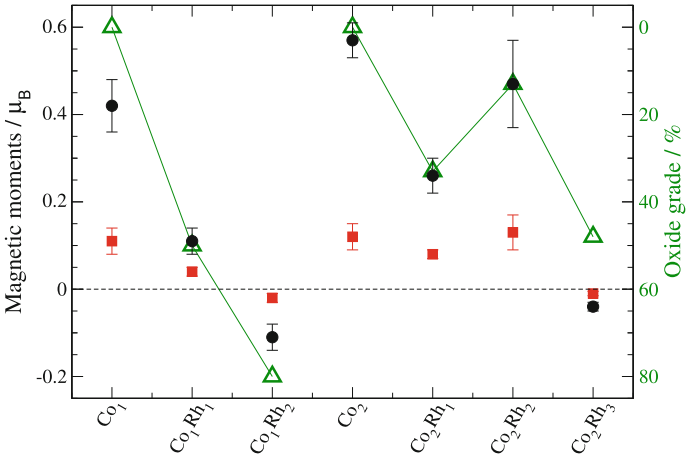

Fig. 7.17 Magnetic moments (left axis, spin •, orbit ■) and degree of oxidation (right axis, ▲) for Co_nRh_m clusters

is increasing up to 80% for Co_1Rh_2. In parallel the magnetic moment is decreasing almost linearly as depicted in Fig. 7.17 and for Co_1Rh_2−O similar to CoPd−O an antiferromagnetic coupling is observed [55].

The situation is more complicated for Co_2Rh_m. In general an increased chemical reactivity is found for these alloy clusters, however, in a non-monotonic way. Adding a Rh atom to the Co dimer results in an oxidation rate of 30% and a decreased magnetic moment, whereas a second Rh atom reduces oxidation to 13% and a third Rh atom increases it again up to 48%. The increased oxidation rate is correlated to a reduction of the magnetic moment of the Co atoms and a transition from a ferromagnetic to an antiferromagnetic alignment of the Co magnetic moments.

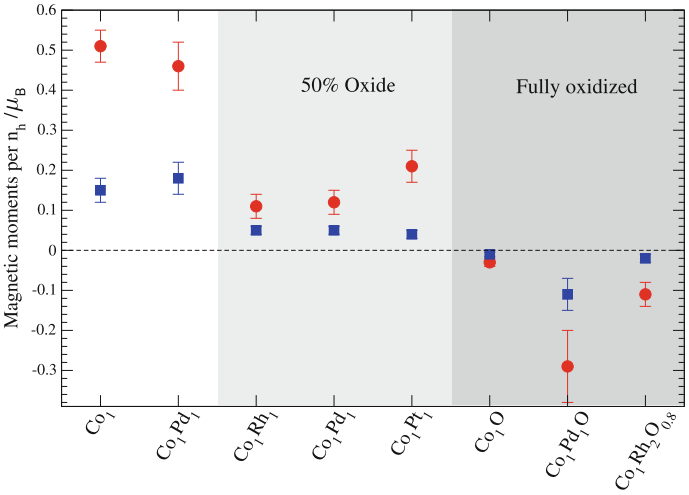

Fig. 7.18 Co spin (circle ●) and orbital (square ■) magnetic moments of Co_1M_m adatoms and alloy clusters depending on the oxidation. Note, that the oxidation grade of Co_1Rh_2 is only 80%

Table 7.1 Magnetic moment of Co_nX_1-O clusters on Ni/Cu(100)

Cluster	Oxide	μ_s	μ_ℓ	μ_ℓ/μ_s
Co_1Rh_1	50	0.11	0.04	0.32
Co_1Pd_1	40	0.12	0.05	0.37
Co_1Pt_1	50	0.21	0.04	0.17
Co_2Rh_1	33	0.26	0.08	0.30
Co_2Pt_1	≅50	0.24	0.09	0.38

For Rh atoms XMCD spectra can be recorded at the Rh $M_{2,3}$ edges similar to the 3d metal $L_{2,3}$ edges. However, as the Auger rates of the Rh 3p core holes are much larger due to the possible super-Coster-Kronig decay and the 3p-4d dipole matrix element is smaller, the measurement of the corresponding XAS and XMCD spectra of the diluted cluster samples is challenging [48]. Hence, only for the Rh rich cluster samples Co_1Rh_2 and Co_2Rh_3 XMCD spectra have been recorded [55].

Co_1Rh_2 clusters do not show any dichroism, whereas for Co_2Rh_3 an XMCD signal is found. From the negative sign of the XMCD at the Rh M_3 edge it can be concluded, that the Rh magnetic moment is ferromagnetically oriented relative to the Ni substrate and antiferromagnetically to the Co adatoms. This may result in a complex non-collinear coupling within the cluster which would explain the small magnetic moments found for the Co atoms (Fig. 7.18).

In Table 7.1 the magnetic moments of some oxidised Co clusters are summarised. Comparing the spin moments to the unoxidised alloy clusters or the Co_n clusters only a reduction of the spin moment is found. Co_1X_1-O clusters for Rh and Pd show very similar values for the spin and orbital moments of $\mu_s \cong 0.1$ and $\mu_\ell \cong 0.04$.

For Pt the orbital moment has the same value, but the spin moment is twice as large for the same amount of oxidation in the order of 50%. For Co_1Pd_1-O an antiferromagnetic alignment of the Co moment relative to the Ni surface is found and for Co_2Rh_3-O clusters a non-collinear coupling is proposed, as the Co and Rh is coupled antiferromagnetically.

Comparing the results of the magnetic properties for the differently oxidised Co alloy clusters one can conclude, that the oxidation of the Co cluster results in a reorientation of the magnetic moment of the Co atoms within the cluster relative to the magnetised surface. For the Rh atoms in Co_2Rh_3-O a ferromagnetic orientation of the magnetic moments is found, whereas the Co moments are strongly suppressed. Hence, oxygen mainly influences the Co atoms, whereas Rh and possibly also Pd atoms are less affected. The observation of a ferromagnetic ordering of small Ru clusters, which can also be expected for Rh clusters and is observed for Co_2Rh_3-O, supports this conclusion.

7.6 Summary

To summarise, the magnetic properties of adatoms and small mass selected 3d metal and alloy clusters have been studied using soft X-rays. By using the unique possibility of magnetic circular dichroism to measure the orbital and spin magnetic moments detailed information on the magnetic properties have been obtained on the very small particles in the few atom limit.

The magnetic moments show a strong dependency on the size and composition of the deposited clusters, which proves that size selection is important and each atom counts.

A non-collinear coupling is found for small Cr_n clusters with the help of calculations based on the SPR-KKR method. The magnetic coupling depends strongly on the size and the chosen magnetised surface which can be understood by the spin frustration of the magnetic moments and the variation of the exchange coupling constants J.

For Co clusters with up to three atoms per cluster a ferromagnetic coupling relative to the magnetised surface and also within the cluster is found, which is the case if the cluster is alloyed with a 4d or 5d metal. The alloying has a strong effect on the magnetic moments of the Co atoms, however, there is also a very strong increase of the chemical reactivity of the alloy cluster against oxidation.

The oxidation results in general in a strong decrease of spin and orbital moments of the Co atoms within the cluster and for CoO a switch to an antiferromagnetic coupling of the Co atom relative to the surface is found with very small magnetic moments. This antiferromagnetic coupling is also found for oxidised Co_1Pd_1 and Co_1Rh_2 clusters with much larger magnetic moments compared to CoO.

For some CoRh clusters the magnetic properties could be measured for both, the Co and Rh atoms. Rh shows a much weaker X-ray magnetic circular dichroism effect, nevertheless, again a strong size and composition dependency is found. In

particular, for Co_2Rh_3 an antiferromagnetic orientation of the Rh magnetic moments relative to the surface and small Co magnetic moments are found, which is a hint to a non-collinear coupling also within these alloy clusters.

The studied 3d metal and alloy clusters with only a few atoms do not show any remanent magnetisation, but some clusters show a complex non-collinear magnetic coupling. This non-collinear coupling can be tailored by choosing the right size, composition and substrate material. Hence, these clusters can serve maybe as the smallest model systems for large complex spin structures which are considered for magnetic storage devices.

Acknowledgements This work was supported by the Deutsche Forschungsgemeinschaft via the SFB668 project A7. We thank the BESSY II beamline staff, namely H. Pfau and F.-X. Talon, for their logistic assistance. Finally, we have to thank Graham Appleby for carefully reading the manuscript.

References

1. E. Weschke, H. Ott, E. Schierle, C. Schussler-Langeheine, D.V. Vyalikh, G. Kaindl, V. Leiner, M. Ay, T. Schmitte, H. Zabel, P.J. Jensen, Phys. Rev. Lett. **93**(15), 157204 (2004)
2. P.J. Hsu, A. Finco, L. Schmidt, A. Kubetzka, K. von Bergmann, R. Wiesendanger, Phys. Rev. Lett. **116**, 017201 (2016)
3. G. Binasch, P. Grünberg, F. Saurenbach, W. Zinn, Phys. Rev. B **39**, 48284830 (1989)
4. P. Grünberg, R. Schreiber, Y. Pang, M.B. Brodsky, H. Sowers, Phys. Rev. Lett. **57**(19), 2442 (1986)
5. R.E. Camley, J. Barnas, Phys. Rev. Lett. **63**, 664 (1989)
6. N. Romming, C. Hanneken, M. Menzel, J.E. Bickel, B. Wolter, K. von Bergmann, A. Kubetzka, R. Wiesendanger, Science **341**(6146), 636639 (2013)
7. P. Gambardella, S. Rusponi, M. Veronese, S.S. Dhesi, S. Rusponi, M. Veronese, S.S. Dhesi, P.H. Dederichs, K. Kern, C. Carbone, H. Brune1, Science **300**, 1130 (2003)
8. M. Toshio, S. Tobias, M. Tobias, B. Christopher, B. Timofey, S. Alexander, K. Christian, A. Stephan, M. Michael, H. Martin, G. Matthias, O. Sergey, H. Wolfram, M. Ingrid, S. Gerd, E. Arthur, W. Wulf, Nature **503**(7475), 242246 (2013)
9. H. Brune, P. Gambardella, Surf. Sci. **603**(1012), 18121830 (2009)
10. I.G. Rau, S. Baumann, S. Rusponi, F. Donati, S. Stepanow, L. Gragnaniello, J. Dreiser, C. Piamonteze, F. Nolting, S. Gangopadhyay, O.R. Albertini, R.M. Macfarlane, C.P. Lutz, B.A. Jones, P. Gambardella, A.J. Heinrich, H. Brune, Science **344**(6187), 988992 (2014)
11. S. Baumann, F. Donati, S. Stepanow, S. Rusponi, W. Paul, S. Gangopadhyay, I.G. Rau, G.E. Pacchioni, L. Gragnaniello, M. Pivetta, J. Dreiser, C. Piamonteze, C.P. Lutz, R.M. Macfarlane, B.A. Jones, P. Gambardella, A.J. Heinrich, H. Brune, Phys. Rev. Lett. **115**, 237202 (2015)
12. F. Donati, A. Singha, S. Stepanow, C. Wäckerlin, J. Dreiser, P. Gambardella, S. Rusponi, H. Brune, Phys. Rev. Lett. **113**, 237201 (2014). https://doi.org/10.1103/PhysRevLett.113.237201
13. T. Eelbo, M. Waniowska, P. Thakur, M. Gyamfi, B. Sachs, T.O. Wehling, S. Forti, U. Starke, C. Tieg, A.I. Lichtenstein, R. Wiesendanger, Phys. Rev. Lett. **110**, 136804 (2013). https://doi.org/10.1103/PhysRevLett.110.136804
14. M. Etzkorn, C.F. Hirjibehedin, A. Lehnert, S. Ouazi, S. Rusponi, S. Stepanow, P. Gambardella, C. Tieg, P. Thakur, A.I. Lichtenstein, A.B. Shick, S. Loth, A.J. Heinrich, H. Brune, Phys. Rev. B **92**, 184406 (2015). https://doi.org/10.1103/PhysRevB.92.184406
15. A. Lehnert, S. Rusponi, M. Etzkorn, S. Ouazi, P. Thakur, H. Brune, Phys. Rev. B **81**, 104430 (2010). https://doi.org/10.1103/PhysRevB.81.104430
16. U. Heiz, A. Sanchez, S. Abbet, W.D. Schneider, J. Am. Chem. Soc. **121**, 32143217 (1999)

17. A. Sanchez, S. Abbet, U. Heiz, W.D. Schneider, H. Häkkinen, R.N. Barnett, U. Landman, J. Phys. Chem. A **103**, 9573 (1999)
18. J. Lau, A. Föhlisch, M. Martins, R. Nietubyč M. Reif, W. Wurth. New J. Phys. **4**, 98 (2002)
19. J. Lau, A. Föhlisch, R. Nietubyč, M. Reif, W. Wurth. Phys. Rev. Lett. **89**(5), 057201 (2002)
20. P. Bruno, Phys. Rev. B **39**, 865868 (1989)
21. P. Bruno, J.P. Renard, Appl. Phys. A **49**(5), 499506 (1989)
22. J. Stöhr, J. Elec. Spec. Relat. Phenom. **75**, 253272 (1995)
23. J. Lau, A. Achleitner, H.U. Ehrke, U. Langenbuch, M. Reif, W. Wurth, Rev. Sci. Instr. **76**, 063902 (2005)
24. H.P. Cheng, U. Landman, J. Phys. C **98**, 35273537 (1994)
25. H. Cheng, U. Landman, Science **260**, 1304 (1993)
26. J. Stöhr, J. Magn. Magn. Mat. **200**, 470497 (1999)
27. J. Stöhr, H.C. Siegmann, *Solid-State Sciences*, vol. 5 (Springer, Berlin, 2006)
28. D.H. Bilderback, P. Elleaume, E. Weckert, J. Phys. B **38**(9), S773 (2005)
29. S. Sasaki, K. Miyata, T. Takada, Jpn. J. Appl. Phys. **31**, L1794 (1992)
30. B.T. Thole, P. Carra, F. Sette, G. van der Laan, Phys. Rev. Lett. **68**(12), 1943 (1992)
31. C.T. Chen, Y.U. Idzerda, H.J. Lin, N.V. Smith, G. Meigs, E. Chaban, G.H. Ho, E. Pellegrin, F. Sette, Phys. Rev. Lett. **75**(1), 152 (1995)
32. R. Wu, A.J. Freeman, Phys. Rev. Lett. **73**(14), 1994 (1994)
33. O. ipr, J. Minr, H. Ebert, EPL (Europhys. Lett.) **87**(6), 67007 (2009)
34. C. Piamonteze, P. Miedema, F.M.F. de Groot, Phys. Rev. B **80**, 184410 (2009)
35. A. Scherz, H. Wende, K. Baberschke, J. Minar, D. Benea, H. Ebert, Phys. Rev. B **66**, 184401 (2002)
36. A. Scherz, H. Wende, K. Baberschke, Appl. Phys. A **78**, 843846 (2004)
37. A. Scherz, H. Wende, C. Sorg, K. Baberschke, J. Minar, D. Benea, H. Ebert, Physica Scripta **T115**, 586588 (2005)
38. S. Lounis, M. Reif, P. Mavropoulos, L. Glaser, P. Dederichs, M. Martins, S. Blügel, W. Wurth, Eur. Phys. Lett. **81**, 47004 (2008)
39. G. Prümper, S. Kröger, R. Müller, M. Martins, J. Viefhaus, P. Zimmermann, U. Becker, Phys. Rev. A **68**, 032710 (2003)
40. M. Martins, K. Godehusen, T. Richter, P. Wernet, P. Zimmermann, J. Phys. B **39**(5), R79R125 (2006)
41. R. Robles, L. Nordstrom, Phys. Rev. B **74**(9), 094403 (2006)
42. W. Wurth, M. Martins, *in Atomic Clusters from Gas Phase to Deposited*, *The Chemical Physics of Solid Surfaces*, vol. 12, ed. by D. Woodruff (Elsevier, Amsterdam, 2007), p. 471
43. M. Martins, W. Wurth, J. Phys. Cond. Mat. **28**, 503002 (2016)
44. S. Lounis, P. Mavropoulos, P.H. Dederichs, S. Blügel, Phys. Rev. B (Condens. Matter Mater. Phys.) **72**(22), 224437 (2005)
45. L. Glaser, K. Chen, S. Fiedler, M. Wellhöfer, W. Wurth, M. Martins, Phys. Rev. B **86**, 075435 (2012)
46. K. Chen, S. Fiedler, I. Baev, T. Beeck, W. Wurth, M. Martins, New J. Phys. **14**(12), 123005 (2012)
47. A.J. Cox, J.G. Louderback, L.A. Bloomfield, Phys. Rev. Lett. **71**(6), 923 (1993)
48. J. Minr, S. Bornemann, S. Mankovsky, H. Ebert, M. Martins, M. Reif, L. Glaser, W. Wurth, Phys. Status Solidi (b) **247**(5), 11801186 (2010)
49. J. Honolka, K. Kuhnke, L. Vitali, A. Enders, K. Kern, S. Gardonio, C. Carbone, S.R. Krishnakumar, P. Bencok, S. Stepanow, P. Gambardella, Phys. Rev. B (Condens. Matter Mater. Phys.) **76**(14), 144412 (2007)
50. N.A. Frey, S. Sun, *Inorganic Nanoparticles: Synthesis, Application, and Perspective* (2010), p. 3368
51. I. McFadyen, E. Fullerton, M. Carey, Mrs Bull. **31**(05), 379383 (2006)
52. G.W. Qin, Y.P. Ren, N. Xiao, B. Yang, L. Zuo, K. Oikawa, Int. Mater. Rev. **54**(3), 157179 (2009)

53. A.A. Khajetoorians, B. Baxevanis, C. Hübner, T. Schlenk, S. Krause, T.O. Wehling, S. Lounis, A. Lichtenstein, D. Pfannkuche, J. Wiebe, R. Wiesendanger, Science **339**(6115), 5559 (2013)
54. K. Chen, T. Beeck, S. Fiedler, I. Baev, W. Wurth, M. Martins, Phys. Rev. B **93**, 144421 (2016)
55. T. Beeck, I. Baev, K. Chen, S. Palutke, W. Wurth, M. Martins, New J. Phys. **18**(11), 113007 (2016)
56. A. Kleibert, J. Passig, K.H. Meiwes-Broer, M. Getzlaff, J. Bansmann, J. Appl. Phys. **101**(11), 114318 (2007)
57. J. Bansmann, A. Kleibert, F. Bulut, M. Getzlaff, P. Imperia, C. Boeglin, K.H. Meiwes-Broer, Eur. Phys. J. D **45**(3), 521528 (2007)
58. J. Bansmann, M. Getzlaff, A. Kleibert, F. Bulut, R. Gebhardt, K. Meiwes-Broer, Appl. Phys. A **82**(1), 7379 (2006)
59. F. Tournus, A. Tamion, N. Blanc, A. Hannour, L. Bardotti, B. Prvel, P. Ohresser, E. Bonet, T. Epicier, V. Dupuis, Phys. Rev. B **77**(14), 144411 (2008)
60. W. Grange, I. Galanakis, M. Alouani, M. Maret, J.P. Kappler, A. Rogalev, Phys. Rev. B **62**(2), 11571166 (2000)
61. W. Grange, M. Maret, J.P. Kappler, J. Vogel, A. Fontaine, F. Petroff, G. Krill, A. Rogalev, J. Goulon, M. Finazzi, N.B. Brookes, Phys. Rev. B **58**(10), 62986304 (1998)
62. B.T. Thole, G. van der Laan, Phys. Rev. B **38**(5), 3158 (1988)
63. G. van der Laan, B.T. Thole, Phys. Rev. Lett. **60**(19), 19771980 (1988)
64. C. Antoniak, M. Spasova, A. Trunova, K. Fauth, F. Wilhelm, A. Rogalev, J. Minr, H. Ebert, M. Farle, H. Wende, J. Phys.: Condens. Matter **21**(33), 336002 (2009)
65. C. Antoniak, J. Lindner, M. Spasova, D. Sudfeld, M. Acet, M. Farle, K. Fauth, U. Wiedwald, H.G. Boyen, P. Ziemann, F. Wilhelm, A. Rogalev, S. Sun, Phys. Rev. Lett. **97**(11), 117201 (2006)
66. A. Kleibert, K.H. Meiwes-Broer, J. Bansmann, Phys. Rev. B **79**(12), 125423 (2009)
67. M. Reif, L. Glaser, M. Martins, W. Wurth, Phys. Rev. B **72**, 155405 (2005)